The EMBO Journal Vol.18 No.6 pp.1447–1458, 1999

X-ray structure of T4 endonuclease VII: a DNA junction resolvase with a novel fold and unusual domain-swapped dimer architecture

Hans Raaijmakers, Olivier Vix[1], Imre Törõ, Stefan Golz[2], Börries Kemper[2] and Dietrich Suck[3]

Structural Biology Programme, EMBL, Meyerhofstrasse 1, D-69117 Heidelberg and [2]Institut für Genetik, Universität Köln, Zülpicherstrasse 47, D-50674 Köln, Germany

[1]Present address: Synthelabo Biomoleculaire, Biologie Structurale, 16, rue d'Ankara, F-67080 Strasbourg Cedex, France

[3]Corresponding author
e-mail: suck@embl-heidelberg.de

Phage T4 endonuclease VII (Endo VII), the first enzyme shown to resolve Holliday junctions, recognizes a broad spectrum of DNA substrates ranging from branched DNAs to single base mismatches. We have determined the crystal structures of the Ca^{2+}-bound wild-type and the inactive N62D mutant enzymes at 2.4 and 2.1 Å, respectively. The Endo VII monomers form an elongated, highly intertwined molecular dimer exhibiting extreme domain swapping. The major dimerization elements are two pairs of antiparallel helices forming a novel 'four-helix cross' motif. The unique monomer fold, almost completely lacking β-sheet structure and containing a zinc ion tetrahedrally coordinated to four cysteines, does not resemble any of the known junction-resolving enzymes, including the *Escherichia coli* RuvC and λ integrase-type recombinases. The S-shaped dimer has two 'binding bays' separated by ~25 Å which are lined by positively charged residues and contain near their base residues known to be essential for activity. These include Asp40 and Asn62, which function as ligands for the bound calcium ions. A pronounced bipolar charge distribution suggests that branched DNA substrates bind to the positively charged face with the scissile phosphates located near the divalent cations. A model for the complex with a four-way DNA junction is presented.

Keywords: DNA junction resolvase/domain swapping/T4 endonuclease VII/X-ray structure

Introduction

The recognition and resolution of DNA junctions is an essential step in DNA recombination and repair, and proteins binding to and resolving these junctions have been found in all kingdoms of life (West, 1993; Kemper, 1997; White *et al*., 1997). Endonuclease VII (Endo VII), a 157 amino acid product of gene 49 of bacteriophage T4, expressed at early and late stages of infection from different promoters, is the prototypic junction-resolving enzyme, since it was the first enzyme shown to resolve Holliday junctions (Mizuuchi, 1982). Endo VII has been shown to be involved in mismatch repair; however, its major function *in vivo*, at least in the late stages of phage infection, appears to be the resolution of branchpoints prior to packaging of the DNA into the phage head (Kemper and Brown, 1976; Solaro *et al*., 1993; Grebenshchikova *et al*., 1994). Phages mutated in gene 49 are defective in packaging their newly synthesized DNA and accumulate highly branched DNA molecules.

In contrast to other resolvases, such as, for example, yeast CCE1 or *Escherichia coli* RuvC, Endo VII has a broad substrate specificity and recognizes a variety of branched DNA structures and/or structural perturbations in DNA. Besides Holliday junctions and cruciform DNA, Endo VII will not only cleave Y-junctions, heteroduplex loops, single-stranded overhangs and curved DNA, but also abasic sites and single base mismatches (Kemper *et al*., 1990; Kemper, 1997; Greger and Kemper, 1998). Mismatch cleavage by Endo VII has been exploited successfully for screening for mutations (Youil *et al*., 1995).

It has been suggested that the inclination of the DNA helix segments on either side of the branchpoint is important for recognition by Endo VII; however, the fact that single base mismatches and abasic sites are cleaved efficiently puts a question mark over this hypothesis (Bhattacharyya *et al*., 1991). Furthermore, comparative gel mobility experiments indicate a global structural change of four-way junctions on binding to Endo VII (Pöhler *et al*., 1996). Therefore, structural studies are required to understand the mechanism underlying the structural selectivity of Endo VII.

Endo VII is active as a dimer and nicks both strands in a divalent cation-catalyzed reaction 2–6 bp 3′ of the branchpoint in independent, but temporally closely correlated reactions (Pottmeyer and Kemper, 1992). For a supercoil-stabilized cruciform substrate, it was shown that the two strands of the junction are cleaved within the lifetime of the enzyme–junction complex (Giraud-Panis and Lilley, 1997). On the other hand, the time delay between nick and counternick of mismatches is such that it allows for the repair by DNA polymerase and ligase *in vitro* (Solaro *et al*., 1993). This has led to the conjecture that Endo VII primarily acts as a repair enzyme and represents a member of an ancient class of broad specificity repair enzymes (Kemper, 1997).

While Endo VII, like other resolvases, is active as a dimer, higher order complexes with cruciform DNA containing two or even three protein dimers per junction have been observed in band shift assays, electron micrographs and gel chromatography experiments (Golz *et al*., 1997; Kupfer *et al*., 1998; I.Törõ and D.Suck, unpublished observations). At present, it is not known whether these complexes are *in vitro* artefacts or whether they have any biological meaning.

The cleavage pattern and the relative cleavage efficiencies of Endo VII are influenced by the local base sequence (Pottmeyer and Kemper, 1992); however, other resolvases display a more pronounced sequence specificity. For example, the yeast CCE1 protein shows a strong preference for cutting 3′ to a CT (Schofield *et al*., 1998).

Endo VII shows little sequence homology to other resolvases and, as a unique feature, contains one zinc ion per monomer, coordinated to four cysteines, which is essential for stabilizing the fold (Giraud-Panis *et al*., 1995). The relevance of significant sequence homology of the N-terminal 62 residues (containing the cysteines) with gp59 from mycobacteriophage L5 and of a 30 amino acid stretch near the C-terminus with endonuclease V from phage T4 is not clear.

We present here the high resolution crystal structures of Ca^{2+}-bound wild-type and the inactive N62D mutant of phage T4 Endo VII. The implications of its unique fold and highly unusual domain-swapped dimer architecture for the catalytic mechanism and the interaction with branched DNA are discussed, and a model of a complex with a four-way DNA junction is presented.

Results and discussion

The crystal structure of the N62D mutant was determined first by MIRAS techniques using a seleno-methionine-labeled protein as the major source for phase determination at high resolution. The mercury and gold derivatives were used to locate nine out of 10 selenium atoms in an anomalous difference Fourier. The resulting electron density map was of excellent quality (see Figure 5), allowing chain tracing and model building of the complete Endo VII dimer present in the asymmetric unit. Hindering the X-ray analysis of the wild-type protein was severe non-isomorphism for many of the derivatives obtained by soaking, which often also led to a change in space group. In contrast to the catalytically inactive N62D mutant, the expression of the seleno-methionine-labeled wild-type Endo VII proved to be very difficult. Significant conformational changes in the mutant compared with the wild-type protein precluded the determination of the wild-type structure by simple molecular replacement and, therefore, SIRAS phasing based on a mercury derivative had to be applied. The wild-type and mutant Endo VII structures were refined to *R*-factors of 25.3 and 21.3% at 2.4 and 2.1 Å, respectively. Refinement statistics of the final models are summarized in Table I.

Table I. Refinement statistics of the final model

	Wild-type	N62D
Resolution range (Å)	18–2.4	27–2.1
No. of reflections used in refinement	16 359	24 998
Reflections used in R_{free} calculations (%)	5	5
No. of protein atoms	2×1272	2×1272
No. of zinc atoms	2	2
No. of water molecules	63	262
No. of sulfate molecules	–	12
No. of calcium atoms	3	–
R-factor (%)	25.3	21.3
R_{free} (%)	30.9	26.2
R.m.s.d. from ideal stereochemistry		
Bond lengths (Å)	0.028	0.019
Bond angles (°)	3.20	2.13
Mean *B*-factor (Å^2)	48.9	29.3
Main chain (Å^2)	48.3	25.8
Side chain (Å^2)	49.8	30.1
Solvent (Å^2)	42.1	39.6
Ramachandran plot		
Residues in most favored regions (%)	93.6	95.7
Residues in additionally allowed regions (%)	6.4	4.3
Residues in generously allowed regions (%)	0.0	0.0
R.m.s.d. NCS-related aoms		
C_α trace (Å)	0.476	0.503
All (Å)	1.15	0.976

Side chains belonging to wild-type chain A: E123, L129, E137, K150; and wild-type chain B: K6, E122, K150, K157 are invisible at 0.8σ.

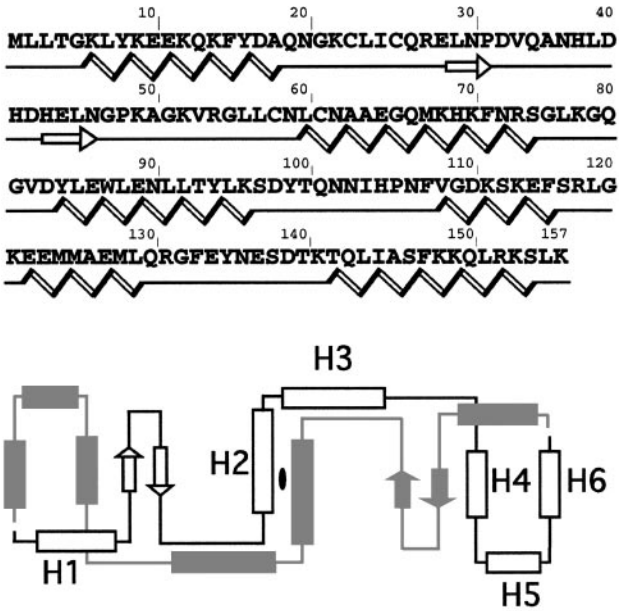

Fig. 1. Top, amino acid sequence and secondary structure assignment of Endo VII. Bottom, topology diagram of the dimer. The helices are numbered H1–H6, the hairpin structure containing the two short β-strands is referred to as 'β-finger' in the text.

Endo VII architecture: a domain-swapped dimer built from unstable monomers

The fold of Endo VII revealed by our X-ray analysis is novel and shows several unusual features not resembling any of the known structures of junction-resolving enzymes. The structure of the individual 157 amino acid Endo VII monomer does not represent a stable fold, as it exposes many hydrophobic residues in its central region and contains two completely separated, flexibly linked domains. They consist of a 60 residue N-terminal domain and a 50 residue C-terminal domain, which are separated by ~50 Å and are connected by a central helix–loop–helix motif (residues 60–96) and an extended chain segment (residues 97–106) (Figures 1 and 2). The C-terminal domain comprising helices 4, 5 and 6 is a compact entity, while the N-terminal domain composed of helix 1, a loop region and a 'β-finger' displays a less compact structure whose integrity critically depends on the presence of a zinc ion. The 'β-finger' formed by residues 38–56 is a hairpin structure containing a four residue stretch of antiparallel β-sheet, the only β-sheet structure found in Endo VII. The zinc ion is tetrahedrally coordinated to

four cysteines located at the N-terminus of helix 2 (C58 and C61) and within the loop region (C23 and C26), which is thereby firmly tethered to the rest of the molecule (Figure 2). In keeping with the critical structural role of the zinc ions, cysteine mutants interfering with zinc binding were found to be inactive (Giraud-Panis *et al*., 1995).

Two extensively intertwined Endo VII monomers related by a non-crystallographic 2-fold axis form an elongated dimer of approximate dimensions 93×45×25 Å (Figure 2). Within the dimer, the C-terminal domain of one monomer interacts with the N-terminal domain of the other monomer, resulting in an extreme case of domain swapping. The C-terminal domain of the 'top' molecule (shown in red in Figure 2A) is located at the 'bottom' end of the dimer and vice versa. N- and C-terminal domains mutually stabilize each other and their orientation relative to the rest of the molecule. A lack of this interaction is presumably mainly responsible for the inactivity of N- and C-terminal deletion mutants (Golz *et al*., 1997; Birkenbihl and Kemper, 1998a; see discussion below). Only minor deviations from the local 2-fold symmetry are observed, and C_α positions of corresponding monomers can be superimposed with r.m.s.d. values of ~0.5 Å.

When viewed along the molecular dyad, the EndoVII dimer has an S-shaped stucture with two 'bays' separated by ~25 Å (the distance between the bound Ca^{2+} ions in wild-type Endo VII is 24 Å; Figure 2A). These bays or channels, which are lined by positively charged residues on one face of the dimer, contain a number of residues shown to be essential for activity, including N62, D40, H41 and E65 (Giraud-Panis and Lilley, 1996; Golz *et al*., 1997; R.P.Birkenbihl, unpublished results) as well as the bound calcium ions, clearly suggesting that they harbor the active sites (see discussion below).

In a view perpendicular to the molecular 2-fold axis, Endo VII appears as a very elongated, slightly curved object with a highly bipolar charge distribution (Figure 2A). Predominantly positively charged residues are exposed on the concave face of the dimer, in particular on helices 2, 4 and 6.

The major dimerization element of the Endo VII dimer is formed by the central part of the monomers comprising helices 2 and 3 and the 10 residue loop connecting them. The arrangement of these helices relative to the molecular 2-fold axis gives rise to the formation of a 'four-helix cross' with two pairs of antiparallel helices crossing each other at an angle of ~70–80° (Figure 2). This highly unusual dimerization motif is reminiscent of the dimer interface in the recently determined structure of an *E.coli* RNA polymerase α subunit domain (Zhang and Darst, 1998). Numerous, mostly hydrophobic residues interacting with their symmetry-related counterparts form an extended hydrophobic core stabilizing the dimer (Figure 2B). The W87R mutant, which directly interferes with these interhelical contacts, has lost its ability to dimerize and, as a consequence, shows neither DNA-binding nor cleavage activity (Birkenbihl and Kemper, 1998b).

Differences between the wild-type and N62D mutant structures

The structure of Endo VII was solved originally using crystals of the N62D mutant grown at acidic pH (4.5) in the presence of 20 mM Mg^{2+} ions (see Materials and methods), while suitable crystals of the wild-type protein were obtained at pH 8.2 in the presence of high concentrations of Ca^{2+} (200 mM). Both magnesium and calcium ions catalyze the resolution activity of the enzyme (S.Pottmeyer and B.Kemper, unpublished results); however, under the crystallization conditions used, no magnesium ions were found to be bound at the active site of the mutant. A comparison of the two structures reveals significant conformational changes (Figure 3) explaining the failure of attempts to solve the wild-type structure by molecular replacement using the refined mutant coordinates. While the overall protein architecture is the same in both structures, there is a significant change in the orientation of the N- and C-terminal domains relative to the central dimerization domain. This leads to a widening of the binding clefts in the mutant and a concomitant increase in the long dimension of the mutant dimer to ~100 Å.

As can be seen in Figure 3B, it is possible to superimpose fairly closely the upper, and also the lower halves of the dimers including the N-terminal domain of one subunit and the C-terminal domain from the other subunit, showing that the relative disposition of these domains is essentially conserved in the wild-type and the mutant protein. The position and orientation of helix 2, however, differ, and a closer inspection of the structures indicates that this helix is bent in wild-type Endo VII around position E65/G66 towards the β-finger and shifted roughly half a helical turn relative to its counterpart (Figure 3C). This narrows the binding cleft compared with the N62D mutant and also affects the packing of the helices, however, without disrupting the hydrophobic core of the dimerization interface. The Ca^{2+} ion directly liganded to D40 and N62 in wild-type Endo VII, which neutralizes the negative charges of the closely spaced carboxylate groups of D40 and E65, could be responsible for these structural changes. The structural rearrangement could also be due to the widely different pH values of crystallization. The close approach of the D40 and E65 carboxylate groups (~3.0 Å) in the N62D mutant suggests that at least one of them is protonated (Figure 3D). This may also account for the fact that no magnesium ions are bound at this site in the mutant. Finally, we cannot entirely exclude that the different packing environments in the two crystal structures are causing conformational changes in the protein.

The structural changes observed in the mutant indicate a certain degree of conformational flexibility of the Endo VII dimer which may be of importance for the interaction with substrates. On the other hand, a comparison of the two structures suggests that the N- and C-terminal domains are fairly rigid entities with a fixed spatial relationship.

Mutants affecting activity and the location of the active site

Extensive site-directed mutagenesis experiments have identified a number of residues affecting dimerization, DNA binding or cleavage (for a review see White *et al*., 1997; B.Kemper, unpublished results). The effects of most of the mutants can be rationalized in terms of the three-dimensional structures and, together with the Ca^{2+}-binding site found in the wild-type protein, allow the identification of the putative active site.

Residues D40, H41, N62 and E65 located in the cleft

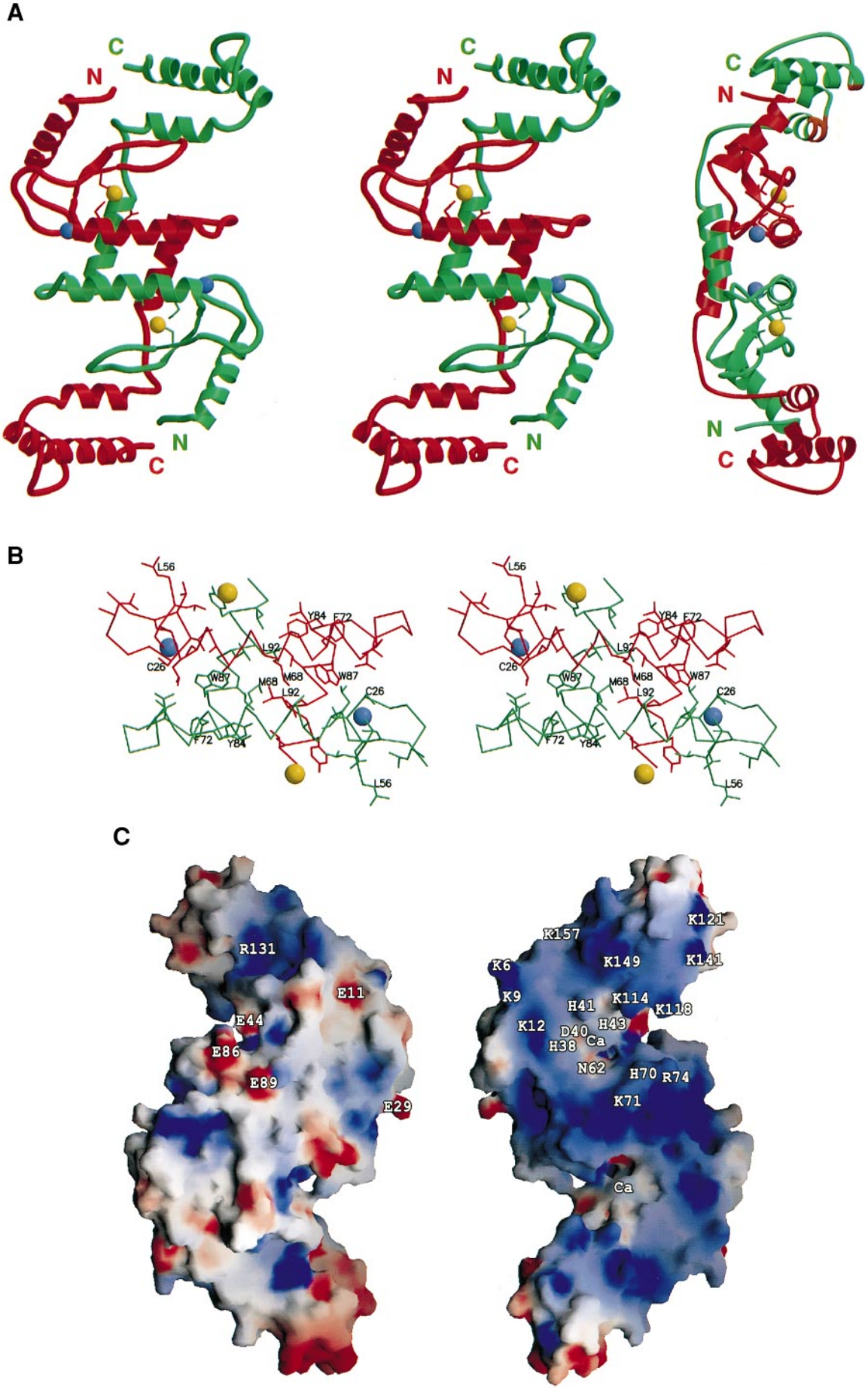
A
C
N
N
C
C
N
N
C
C
N
N
C
B
L56
Y84
F72
L92
C26
W87
M68
M68
W87
L92
C26
F72
Y84
L56
L56
Y84
F72
L92
C26
W87
M68
M68
W87
L92
C26
F72
Y84
L56
C
R131
E11
E44
E86
E89
E29
K157
K121
K6
K149
K141
K9
H41
K114
K118
K12
D40
H43
H38
Ca
N62
H70
R74
K71
Ca

between the β-finger and helix 2 are essential for activity, but not for DNA binding (Giraud-Panis and Lilley, 1996; Golz *et al*., 1997; R.P.Birkenbihl, unpublished results). It is therefore highly likely that the Ca^{2+} ion directly coordinated to D40 and N62 and located close to E65 marks the position of the catalytic cation (Figure 2). A superposition of the putative active site regions in the wild-type and mutant proteins as shown in Figure 3D does not provide a straightforward explanation for the inactivity of the N62D mutant, since no metal ion is bound in the mutant structure and D40 and/or E65 appear to be protonated. In principle, D62 could also function as a ligand for the catalytic cation; however, the charges in the active site cleft may not be balanced properly in the mutant. Another acidic residue, E86, located on the opposite face of the dimer and pointing into the solvent, has been reported to be catalytically essential (Pöhler *et al*., 1996). The reason for the apparent inactivity of an E86A mutant is not obvious from the three-dimensional structure (Figure 2), unless one assumes that the mutation somehow interferes with the proper folding of the protein.

Other critical residues including W87 and F72 are part of the hydrophobic four-helix cross dimerization interface (Figure 2B). The W87R and F72S mutants will clearly disrupt this interface and, as one would expect, show neither dimer formation nor activity (Birkenbihl and Kemper, 1998b).

As mentioned above, zinc ions are essential for the integrity of the fold by tethering the loop between helix 1 and the β-finger to the N-terminus of helix 2 (Figure 2) and, accordingly, the C23S and C61S mutants which no longer bind zinc are inactive (Giraud-Panis *et al*., 1995). The inner two zinc ligands (C26 and C58) seem to be redundant to a certain extent since they still retain some zinc-binding ability if either cysteine is mutated into a serine.

Deletions at either the C- or N-terminus severely affect DNA binding and activity, and mutants lacking residues 1–10 or 151–157 are inactive (Golz *et al*., 1997; Birkenbihl and Kemper, 1998a). The effect of these mutations will be two-fold: firstly, a disruption of the stabilizing interaction between the N-terminal domain of one monomer with the C-terminal domain of the other monomer, which will also affect their relative orientation to the rest of the molecule; and secondly, a loss of positively charged residues which may be important for DNA binding. In agreement with the three-dimensional structure is the observation that the individually inactive N62D and the C-terminal Δ151–157 deletion mutant can complement each other to form an active heterodimer (Golz *et al*., 1997). One half of this heterodimer will have a wild-type active site with correct interactions of intact N- and C-terminal domains.

Comparison with RuvC and other junction-resolving enzymes

A number of junction-resolving enzymes from various organisms have been studied in detail by biochemical and various biophysical techniques (for reviews see, for example, Kemper, 1997; White *et al*., 1997), but structural data are available for only very few of these enzymes including the *E.coli* RuvC protein and some λ integrase-type recombinases which form and resolve a Holliday junction intermediate during site-specific recombination (Ariyoshi *et al*., 1994; Guo *et al*., 1997; Hickman *et al*., 1997; Kwon *et al*., 1997; Subramanya *et al*., 1997).

There is rarely any sequence homology detectable between Endo VII and other junction resolvases. As noted before by Giraud-Panis *et al*. (1995), a database search reveals significant homology only for the N-terminal section (residues 1–62) containing the zinc-binding cysteines with some proteins including gp59 from mycobacteriophage L5, and for a 30 residue section near the C-terminus (residues 115–145) with T4 endonuclease V, a UV dimer excision-repair enzyme. The significance of these limited sequence homologies is not clear, particularly since in the case of endonuclease V whose three-dimensional structure is known (Vassylyev *et al*., 1995), no structural homology is present in this region. Likewise, the claimed moderate homology of a central 45 amino acid section with T7 endonuclease I, a functionally somewhat related resolvase which, however, cleaves 5′ to the junction in the continuous strands, may not be meaningful.

Escherichia coli RuvC resolves Holliday junctions, the central intermediates of genetic recombination, by cleaving the continuous strands to generate the recombinant DNA molecules (Iwasaki *et al*., 1991; Bennett and West, 1995a). Like Endo VII, it requires divalent cations and is active as a dimer, but otherwise the two proteins show very little homology, in terms of both sequence and structure. As revealed by the X-ray structure determination by Ariyoshi *et al*. (1994), the slightly larger RuvC protein (172 residues) has a fold very different from that of Endo VII at the monomer level. It is a typical αβ-protein with a central five-stranded β-sheet surrounded by helices displaying a topology closely related to that of *E.coli* RNase H1 (Katayanagi *et al*., 1990). In contrast, Endo VII almost completely lacks β-sheet structure and does not contain a stable fold at the monomer level.

The RuvC dimer with approximate dimensions 65×40×35 Å is far less elongated than the Endo VII dimer and has a far more conventional dimerization interface consisting of a pair of parallel helices without intertwining of the monomers. However, the relative disposition of the catalytic centers, which are separated by ~30 Å, and the bipolar charge distribution are similar, clearly suggesting binding of the Holliday junction to the

Fig. 2. Structure of the wild-type Endo VII dimer. (**A**) Ribbon plot representation produced with MOLSCRIPT (Kraulis, 1991) in two perpendicular views (one of them in stereo) with the individual monomers colored red and green. The bound zinc and calcium ions are shown as blue and yellow spheres, respectively. Indicated in ball and stick representation are the side chains of D40 and N62 liganding the calcium as well as the nearby E65. (**B**) Stereo representation of the four-helix cross region showing the hydrophobic residues. They form an extended hydrophobic core representing the major dimerization element of the Endo VII dimer. (**C**) Electrostatic surface representation of the Endo VII dimer. The two opposite faces of the dimer, viewed approximately along the dyad, show a distinctly different charge distribution. The predominantly positively charged face shown on the right (indicated by the blue color) also contains the bound calcium ion and residues known to be essential for activity. The figure was produced with GRASP (Nicholls *et al*., 1991) with the scale ranging from –10 (red) to +17 (blue).

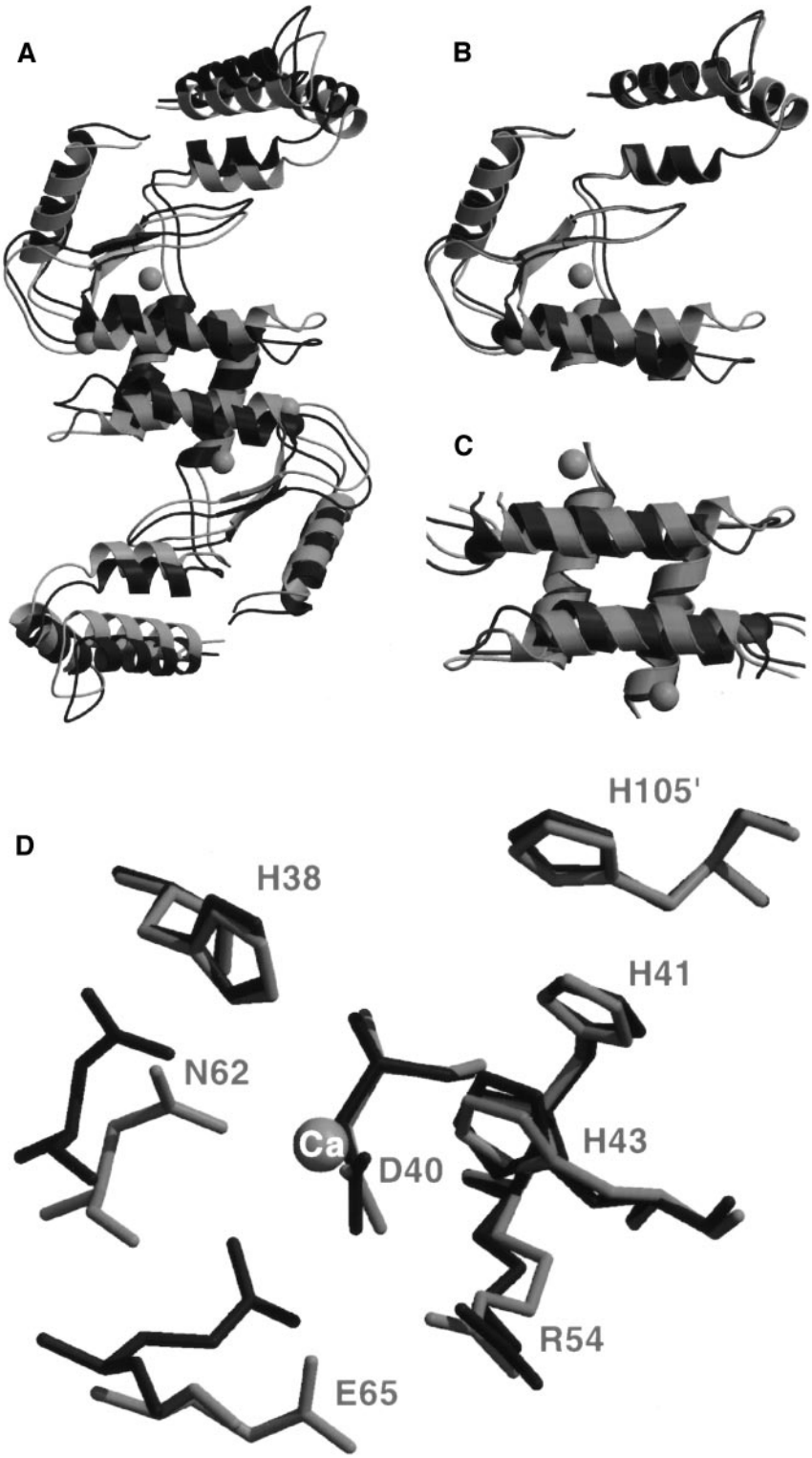

Fig. 3. Superposition of the Endo VII wild-type and N62D mutant structures. (**A**) The orientation of the central four-helix cross relative to the N- and C-terminal domains has changed, leading to a wider cleft between the β-finger and helix 2 in the mutant (shown in black). (**B**) In contrast, the conformation of the N- and C-terminal domains as well as their relative orientation remains essentially the same. (**C**) Helix 2 in the mutant structure is shifted relative to its dyad-related counterpart by about half a helical turn compared with wild-type Endo VII. C_α positions 1–157, 100–157 and 62–96 were used for superposition in (A), (B) and (C), respectively, corresponding to r.m.s.d. values of 2.8, 0.5 and 1.0 Å, respectively. (**D**) Active site superposition of Endo VII wild-type and N62D mutant. The calcium ion bound in the wild-type protein (shown in gray) is liganded to N62 and D40. In the mutant (shown in black), E65 and D40 are in close contact (~3 Å), suggesting that at least one of the carboxylates is protonated. H105′ is contributed by the other monomer.

predominantly positively charged face of the dimer (see discussion below). Four acidic residues essential for activity are found at the active site clefts, three of which are in a disposition closely related to that of the putative active site residues D40, E65 and N62 in Endo VII and the D10, E48 and D70 carboxylates in RNase H1. They presumably represent ligands of the catalytic metal ion and may suggest related catalytic mechanisms for these enzymes. Similar arrangements of acidic residues coordinating the catalytic cation have been found in other Mg^{2+}-dependent nucleases.

Three-dimensional structures are available for several λ integrase-type recombinases including Cre, XerD, HP1, Int and the type I topoisomerase from vaccinia virus, which are all known to resolve Holliday junctions (Guo *et al*., 1997; Hickman *et al*., 1997; Kwon *et al*., 1997; Subramanya *et al*., 1997). However, no significant structural similarity to Endo VII is detectable with any of these enzymes.

Model of an Endo VII–four-way DNA junction complex

Endo VII was the first enzyme shown to resolve Holliday junctions *in vitro* (Mizuuchi *et al*., 1982) and later found to accept as substrates a range of branched DNAs with different structural perturbations. A wealth of data derived from various biophysical and biochemical techniques has since been accumulated concerning the interaction of Endo VII with four-way junctions and other branched DNA molecules (for recent reviews see Kemper, 1997; White *et al*., 1997).

In brief, the following picture has emerged for the binding of Endo VII to a four-way junction, based mainly on comparative gel electrophoresis, protection against hydroxyl radical attack and the analysis of cleavage sites in synthetic cruciform structures with tethered arms. (i) Endo VII binds as a dimer to the minor groove side of a four-way junction, cleaving the exchanging strands in an antiparallel stacked X structure 3′ to the point of strand exchange. (ii) The cleavage reactions of the two strands are independent, but temporally closely correlated, and do occur within the lifetime of the junction–protein complex. (iii) Experiments with a protein A–Endo VII (E86A mutant) fusion construct seem to indicate a change in the global structure of the junction on binding. Other than in the free state, the presence or absence of Mg^{2+} ions does not influence its structure in the bound state.

The pronounced bipolar charge distribution of the Endo VII dimer (Figure 2C) suggests that it binds with its predominantly positively charged face to the minor groove side of the four-way junction, such that the scissile phosphates reach into the 'bays' harboring the catalytic residues and the divalent metal ion, i.e. the Ca^{2+} ion seen in the wild-type enzyme.

Given the 2-fold symmetry of the antiparallel stacked X structure of the junction (in the presence of Mg^{2+} ions) and the 2-fold symmetric distribution of the preferred cutting sites relative to the point of strand exchange, we are assuming that in the complex the molecular dyad of the junction roughly coincides with the molecular 2-fold of the Endo VII dimer.

For docking, we used the coordinates of the antiparallel stacked X structure derived by von Kitzing *et al*. (1990) by computer modeling and extended the arms by regular B-DNA. The RuvA and Cre Holliday junction complexes whose structures have been reported recently (Gopaul *et al*., 1998; Roe *et al*., 1998) cannot be used as models, since they exhibit exact or near square-planar conformations with unstacked bases at the cross-over point which are not compatible with the Endo VII structure and biochemical results. The resulting Endo VII dimer–DNA junction complex is shown in Figure 4. This model has not been refined and thus cannot provide a detailed picture of the interactions, particularly since both the DNA junction and the protein may undergo conformational changes upon binding. Nevertheless, the overall features of the model are in agreement with the available experimental data.

Basic residues exposed on the central helices (residues H70, K71 and R74 on helix 2) could interact with the phosphates of the exchanging strands, and further contacts with the continuous strands are possible involving basic residues located on the helices in the C-terminal domain, in agreement with observed protection patterns (Parson *et al*., 1990). These latter contacts may also explain the observation by Seeman and coworkers (Mueller *et al*., 1990), that immobile junctions with arms shorter than 9 bp are not substrates for Endo VII. To avoid minor steric clashes with the C-terminal domains, the angle between the arms of the X structure junction model derived by von Kitzing *et al*. (1990) may have to be slightly adjusted. In contrast to RuvC and CCE1, where an open structure with unstacked bases at the cross-over point is indicated by hypersensitivity towards permanganate and hydroxyl radicals upon complex formation (Bennett and West, 1995b; White and Lilley, 1997), the footprinting patterns observed with Endo VII suggest a fully stacked conformation consistent with an antiparallel stacked X-structure of the junction.

The two putative active sites in the Endo VII dimer are ~24 Å apart as measured by the distance between the two Ca^{2+} ions bound in the wild-type structure. This has to be compared with a distance of ~23 to ~35 Å between the scissile phosphates (highlighted in yellow in Figure 4) of the preferred cutting sites 2 or 3 bp on either side of the cross-over point. While there is a good match for cuts 2 bp from the cross-over point, a difference of >10 Å is encountered in the case of cutting 3 bp from the junction center. The model suggests that even in the optimal case, due to steric constraints imposed mainly by the central helices (2-fold-related, antiparallel helices 2), it may not be possible simultaneously to position both phosphates correctly with respect to the catalytic residues. This could possibly be achieved by a reorientation of the two arms of the junction contacting the protein, or by a corresponding conformational change in the Endo VII dimer. Alternatively, the junction would have to be reoriented somewhat after the first cut, possibly by a rocking motion, to bring the second phosphate into a productive binding position.

The latter scenario is attractive, since it would explain the asynchrony of bilateral cleavages and the time delay between nick and counter-nick allowing Endo VII to trigger mismatch repair (Solaro *et al*., 1993). It is also fully consistent with the notion that the two cuts do occur within the lifetime of the protein–DNA complex, as has

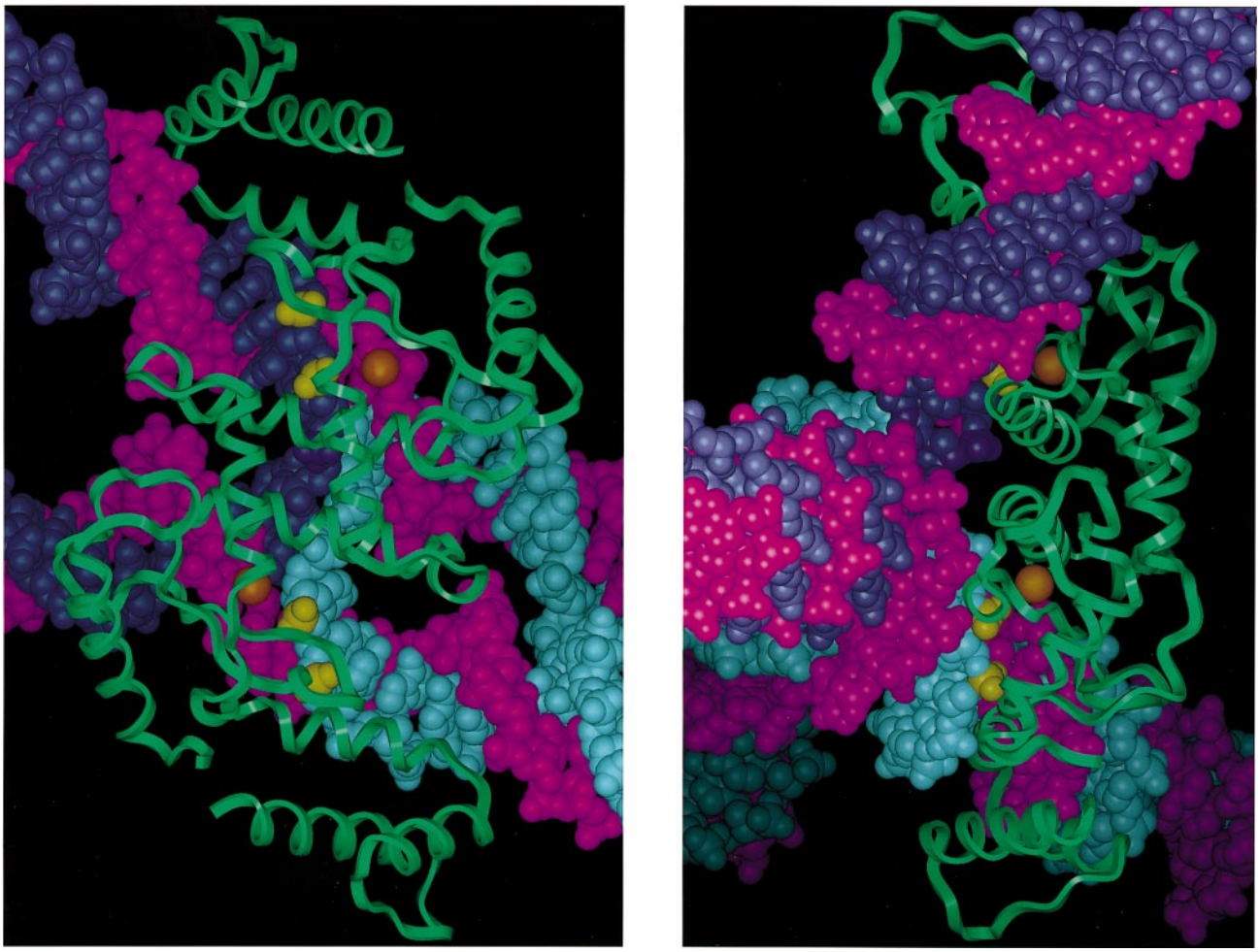

Fig. 4. Model of a four-way DNA junction–Endo VII complex. Two perpendicular views are shown, one approximately along the molecular 2-fold axis of the Endo VII dimer (left), the other one rotated 90° around a vertical axis (right). The Endo VII dimer (represented by a green ribbon) is docked onto the minor groove side of a four-way DNA junction (shown in a space-filled representation) corresponding to the antiparallel stacked X structure (von Kitzing *et al*., 1990). The continuous strands are colored purple, the crossing strands light and dark blue. The scissile phosphates, two and three bases 3′ of the point of strand exchange on the crossing strands, are highlighted in yellow; the calcium ions at the active sites of Endo VII are shown as golden spheres. Minor groove contacts with residues exposed on the central helices as well as major groove contacts with basic residues located in the C-terminal domains can be formed.

been shown for a supercoil-stabilized cruciform substrate (Giraud-Panis and Lilley, 1997).

The cleavage pattern and relative cleavage efficiencies of Endo VII are influenced by the local base sequence (Pottmeyer and Kemper, 1992), although other resolvases, such as CCE1, display a more pronounced sequence selectivity (Schofield *et al*., 1998). This sequence selectivity could be caused by indirect effects of the base sequence on structural parameters of the DNA and/or by direct contacts to the bases likely to occur according to our model in the minor groove around the cross-over point, as well as in the major groove some 8 bp away (Figure 4).

What is the basis for the structural selectivity of Endo VII?

A remarkable feature of Endo VII is its broad substrate specificity already mentioned above, which distinguishes it clearly from cellular resolvases such as RuvC or CCE1. Albeit with differing efficiencies, Endo VII cuts many different kinds of branched DNA species including Holliday junctions, but also DNA containing a single base mismatch or an abasic site. What are the common features of these structural perturbations recognized by the enzyme?

It has been suggested that Endo VII recognizes the inclination of DNA helices, i.e. the angle between the DNA segments on either side of a branchpoint or a structural perturbation (Bhattacharyya *et al*., 1991). This angle is expected to be ~120° in the stacked X conformation of a four-way junction, but also in a three-way junction or bulged DNA containing two additonal adenines. Bent DNA, either intrinsically through the presence of A tracts, or by interaction with a compound, such as in a *cis*-Pt adduct, also appears to be a substrate for Endo VII (Bhattacharyya *et al*., 1991; Murchie and Lilley, 1993). Greger and Kemper (1998) recently have reported that an oligonucleotide with an abasic site, which was demonstrated to be extremely sensitive to cleavage by Endo VII, shows an unusual migration behavior on polyacrylamide gels typical for bent or kinked DNA.

Inspection of the Endo VII binding surface and the proposed model for the four-way junction complex (Figure 4) suggests that the X-ray structure is in general

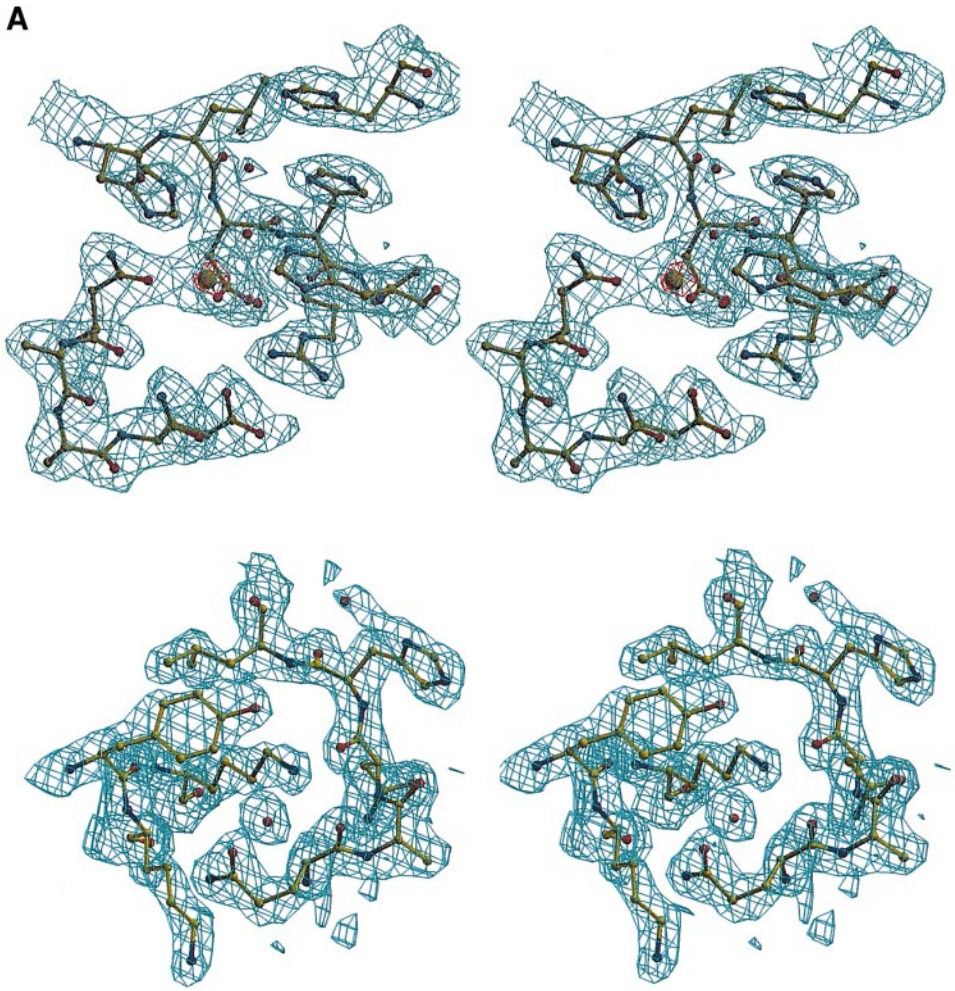

Fig. 5. Portions of the final $2mF_o - DF_c$ map of the wild-type protein around the active site calcium ion, indicated by a larger sphere (**A**), and the experimental map of the N62D mutant near Lys12 (**B**). The contour levels are 1.3σ (blue) and 5.6σ (red) in the wild-type, and 1.3σ in the mutant map. Note the excellent quality of the experimental map of the N62D mutant.

agreement with this hypothesis. However, it does not easily explain the recognition and cleavage of single base mismatches, which, as verified in several X-ray structures, do not display any significant bending. These experimental results seem to indicate that flexibility may be an important parameter in the recognition process, in line with the observation that the stability of a given mismatch (as measured by the melting temperature of the DNA) and cleavage efficiency are correlated reciprocally (Solaro *et al*., 1993). Possibly the lack of flexibility explains why UV-cross-linked thymine dimers containing DNA is not a substrate for Endo VII (B.Kemper, unpublished results).

Endo VII appears to accept as substrates branched DNA with intrinsically inclined helices or DNA which can easily adopt properly inclined configurations. This feature is somewhat reminiscent of the sequence-dependent cleavage by DNase I, which recognizes minor groove width and flexibility of the DNA and preferentially cleaves either where the DNA intrinsically has the proper groove geometry or where it needs the least energy to distort it for productive binding (Suck, 1994, 1998).

Materials and methods

Cloning and expression

The wild-type Endo VII was expressed and purified as described previously (Golz *et al*., 1995), while the N62D mutant (Golz *et al*., 1997) was recloned in vector pET24d to obtain better expression. The N62D mutant was expressed in *E.coli* BL21(DE3)pLys. Overnight pre-cultures on LB plates (30 mg/l kanamycin, 20 mg/l chloramphenicol, 37°C) were used to inoculate one 2 l Erlenmeyer flask each, filled with 800 ml of LB medium (+ antibiotics). After 3 h shaking at 200 r.p.m., 37°C ($OD_{600} \approx 0.8$), the culture was induced with 0.25 mM isopropyl-β-D-thiogalactopyranoside (IPTG). After another 3 h, the cells are harvested, spun down and stored at –80°C.

For the seleno labeling, the protein was expressed in *E.coli* B834 (DE3)pLys, and each pre-culture was used to inoculate 800 ml of M9 medium, supplemented with 50 mg/l of each of the following amino acids: Arg, His, Ile, Leu, Lys, Phe, Thr, Tyr, Val; 20 mg/ml of methionine, 2 mg/l biotin and thiamine, 30 mg/l kanamycin and 20 mg/l chloramphenicol. At the required density ($OD_{600} \approx 0.8$), the cells were spun down, washed twice and dissolved in the same medium, but without methionine. After starvation for 8 h, 40 mg/l L-seleno-methionine was added. After another 2 h, the cells were induced with IPTG for 3 h, spun down and stored at –80°C.

Purification of EndoVII N62D

The frozen cells were thawed and suspended in lysis buffer consisting of 10% glycerol, 10 mM HEPES pH 7.5, 10 mM β-mercaptoethanol,

Table II. Data collection and phasing statistics for the wild-type and N62D mutant crystals

	Wild-type[a]		N62D[b]			
	Native	EMTS[c]	Native	EMTS[c]	$KAu(CN)_2$	Seleno-methionine
X-ray source (λ)	Cu Kα	Cu Kα	Cu Kα	Cu Kα	Cu Kα	BW7B[d] (0.8373 Å)
dmin used (Å)	2.33	2.33	2.1	2.48	3.2	2.0
Observed reflections	59 911	60 492	67 931	24 788	11 272	57 164
Unique reflections	15 953	15 652	21 898	13 736	3287	22 633
Completeness (outer shell) (%)	99.3 (98.2)	99.5 (98.2)	99.9 (99.0)	99.0 (100)	99.3 (100)	99.8 (99.0)
$<I/\sigma(I)>$ (outer shell)	11.8 (3.0)	10.2 (2.8)	7.8 (2.8)	9.4 (7.4)	5.8 (2.4)	10.4 (4.5)
R_{sym}[e]	6.0	6.8	6.9	7.5	17.0	6.5
No. of sites found[f]		2		2	2	9
R_{iso}[g]		29.4		28.0	27.0	28.0
Phasing power[h] (centric/acentric/anomalous)		1.9/2.1/1.5		2.9/3.4/1.7	2.2/2.4/0.76	2.3/3.1/1.3
Figure of merit (solvent-flattened)	0.42 (0.87)		0.55 (0.97)			

[a]Space group C2 a = 145.0 Å, b = 39.4 Å, c = 75.7 Å, β = 106.2°, Z = 8.
[b]Space group $P2_1$ a = 58.0 Å, b = 35.9 Å, c = 92.0 Å, β = 103.9°, Z = 4.
[c]EMTS = ethyl mercury thiosalicylate.
[d]At EMBL outstation Hamburg, DESY.
[e]$R_{sym} = \Sigma|I - <I>|/\Sigma I$.
[f]Excluding the protein-bound Zn ions.
[g]$R_{iso} = \Sigma|F_{PH} - F_P|/\Sigma F_P$.
[h]Phasing power = $<|F_H(calc)|/$phase-integrated lack of closure$>$.

10 mM EDTA, 2 mM Pefablock or phenylmethylsulfonyl fluoride (PMSF), and 450 mM NaCl. The lysate was centrifuged in an ultracentrifuge at 85 000 *g* and the supernatant was loaded onto a Q-Sepharose FF column. After washing with 2 vols of lysis buffer, the protein was eluted by a linear NaCl gradient (200–800 mM) in the following buffer: 10% glycerol, 10 mM HEPES pH 7.5, 10 mM β-mercaptoethanol, 2 mM EDTA.

The peak fractions eluting at ~600 mM NaCl were adjusted to pH 6.5 with MOPS buffer and loaded onto a heparin HiTrap column. A linear gradient of 0.60–1.3 M NaCl in 10 mM MOPS buffer pH 6.5, 10% glycerol, 10 mM β-mercaptoethanol and 2 mM EDTA was applied and Endo VII eluted at 1.1 M NaCl. The purest fractions were concentrated on a Filtron membrane with a 30 kDa cut-off to 12 mg/ml and stored in the presence of 5 mM $ZnCl_2$ and 15 mM $MgCl_2$, 10% glycerol, 10 mM MOPS buffer and 150 mM NaCl. The protein was >99% pure (no other bands visible on silver-stained SDS–PAGE). The yield was ~20 mg/l of LB medium for the native protein and ~10-fold lower for the seleno-methionine derivative. The identity and full incorporation of seleno-methionine were confirmed by mass spectroscopy (MALDI-TOF).

Crystallization and data collection

Wild-type Endo VII was crystallized in hanging drops at 4°C. A 1 µl aliquot of a 16 mg/ml protein solution was mixed with 1 µl of the reservoir solution containing 200 mM $CaCl_2$, 16.5–20% PEG 2K-MME, 100 mM Tris–HCl pH 8.2, 5 mM $ZnCl_2$, 5 mM $(NH_4)_2SO_4$ and 10 mM β-mercaptoethanol. Monoclinic crystals (space group C2, a = 145.0 Å, b = 39.4 Å, c = 75.7 Å, β = 106.2°) containing a dimer in the asymmetric unit appeared overnight and these were used for seeding. The crystals kept growing for ~5 days.

The crystals of Endo VII N62D were also grown by the hanging drop vapor diffusion method at 4°C, using 12 mg/ml protein solution as described above and 15.5–16% PEG 5K-MME in 100 mM NaOAc pH 4.5, 160–250 mM $(NH_4)_2SO_4$, 20 mM $Mg(OAc)_2$, 10 mM β-mercaptoethanol in the reservoir.

A drop equilibrated with a slightly (2% w/v) higher PEG concentration was used to microseed a second drop, which in turn provided macroseeds for the following drops.

Crystals up to 0.8×0.4×0.3 mm have been obtained, but crystals up to 0.3 mm in their longest dimension proved most useful, due to their lower mosaicity. The mutant crystals belong to space group $P2_1$ (a = 58.0 Å, b = 35.9 Å, c = 92.0 Å, β = 103.9°) containing a dimer in the asymmetric unit. Both mutant and wild-type crystals show strongly anisotropic diffraction and mosaicity (varying from 0.45 to 1.35° for the native mutant data set and even higher for the others) which prompted us to choose a lower resolution cut-off than overall I/σ values alone seem to justify (Table II). The seleno-methionine derivative crystals diffracted to 1.6 Å at the BW7B beamline but, due to time constraints, only 2.0 Å data were collected.

All Cu K_α diffraction data were collected using a MAR345 area detector system mounted on an Enraf-Nonius rotating anode generator operating at 40 kV and 90 mA and equipped with nickel-coated focusing mirrors (in-house design). The seleno-methionine derivative data were collected at the EMBL BW7B beamline at the DORIS storage ring, DESY, Hamburg. All data were collected at 100 K using the mother liquor + 20% PEG 400 as a cryoprotectant.

The EMTS and $KAu(CN)_2$ derivatives were obtained by soaking crystals for 1 h in their mother liquor without β-mercaptoethanol and additionally 10% PEG 400 plus 1 mM of the heavy atom compound. In the case of the wild-type protein, only crystals >2 months old survived this treatment. Many of the heavy atom compounds tried caused serious physical damage and/or non-isomorphism. The space groups and cell dimensions were determined and oscillation data were processed using HKL (Otwinowski, 1997) except for the wild-type EMTS derivative data which were processed with XDS98 (Kabsch, 1988) and Scala (CCP4, 1994).

Phasing

The EMTS anomalous difference Patterson function and the EMTS–native isomorphous difference Patterson function were calculated using data from 10 to 3 Å and interpreted manually to obtain the two mercury positions, both in the wild-type and N62D. The gold and mercury were found to bind at the same site in the N62D crystals, sharing two (out of four) cysteine ligands with the protein-bound zinc atom. The wild-type data were phased using the program SHARP (de la Fortelle and Bricogne, 1997) by the SIRAS method with anomalous scattering of the mercury data set.

In the case of the N62D mutant, the MIRAS phases from the gold and mercury derivatives were used to locate the selenium positions in the isomorphous and anomalous difference Fouriers calculated with the seleno-methionine data set. Nine out of 10 expected selenium positions were found. The Zn sites were also very clearly visible (8 and 11σ peaks) in the anomalous difference map. The program SHARP was then used to calculate an electron density map of excellent quality from these four data sets, also using the Zn positions. A solvent content of 52% was assumed for solvent flattening. Two-fold non-crystallographic symmetry (NCS) averaging based on the heavy metal positions was deemed unnecessary. Attempts to solve the structure of the wild-type protein by molecular replacement using the structure of the N62D mutant were not successful.

Model building and refinement

The electron density maps were displayed using the program 'O' (Jones *et al.*, 1991). The sigmaA (CCP4, 1994) weighted 2m $|F_o|$ – D $|F_c|$ map

of N62D was of excellent quality (Figure 5), allowing construction of a complete model of Endo VII N62D, including side chains. The selenium positions were very helpful for tracing the chain. Two clusters containing three closely spaced methionines each (M124, M125, M128) were easily recognized. Another cluster of two selenium atoms near the NCS axis was soon identified as M68, leaving the other selenium site to correspond to one of the N-termini. Tracing the molecule from this N-terminus to the C-terminus was straightforward. The second molecule was traced by applying the NCS operator and was adjusted manually.

The wild-type structure was traced by manually fitting whole helices or strands, from the N62D model, as rigid bodies into the sigmaA-weighted 2m $|F_o|$ – D $|F_c|$ electron density map. A second round of fitting optimized the individual amino acids. The C_α trace was clearly visible, with only a few chain breaks at the 1σ level. Most side chains were also visible.

The structures were refined using the CCP4 suite of programs DM (Cowtan, 1994), REFMAC (Murshodov *et al*., 1997) and ARPP (Lamzin and Wilson, 1993) and validated with PROCHECK (Laskowski *et al*., 1993) and WHATIF (Vriend, 1990). A total of 5% of the reflections have been selected to calculate R_{free}. The starting *R*-factor for the N62D mutant was 0.396 (∞ – 2.1 Å). Individual *B*-factors were restrained but no NCS restraints were applied; nevertheless the monomers differ only marginally (r.m.s.d. = 0.476 Å for the C_α atoms). Arpp was run to find water sites automatically in the later stages of refinement; 262 waters and 12 sulfates were included in the N62D structure.

The starting *R*-factor in the case of the wild-type structure was 0.395 (15–2.5 Å). Individual *B*-factors and NCS were restrained, but residues involved in crystal contacts that were clearly different in omit maps were excluded from NCS restraints. Three calcium ions were included and, additionally, 63 waters were found by Arpp. Seven side chains remained completely disordered. The coordinates have been submitted to the Brookhaven Protein Data Bank.

Acknowledgements

We would like to thank our colleagues Anja Christoph for providing the original clone for the N62D mutant, Hiang Dreher and Gunter Stier for help and advice with the cloning, expression and purification of the proteins, and Yorgo Modis and Joachim Meyer for advice in various computational aspects. We thank Ned Seeman for providing the model coordinates of the four-way DNA junction. We gratefully acknowledge the help of the staff of the EMBL outstation in Hamburg, in particular of Paul Tucker, with data collection at the BW7B beam line. This work was supported by the European Commission through an institutional fellowship to O.V. (contract no. ERBCHBGCT940535). Work in the laboratory of B.K. was supported in part by the Deutsche Forschungsgemeinschaft (DFG Normalverfahren Ke188/12-3) and the Fonds der Chemischen Industrie.

References

Ariyoshi,M., Vassylyev,D.G., Iwasaki,H., Nakamura,H., Shinagawa,H. and Morikawa,K. (1994) Atomic structure of the RuvC resolvase: a Holliday junction-specific endonuclease from *E.coli*. *Cell*, **78**, 1063–1072.

Bennett,R.J. and West,S.C. (1995a) RuvC protein resolves Holliday junctions via cleavage of the continuous (noncrossover) strands. *Proc. Natl Acad. Sci. USA*, **92**, 5635–5639.

Bennett,R.J. and West,S.C. (1995b) Structural analysis of the RuvC–Holliday junction reveals an unfolded junction. *J. Mol. Biol.*, **252**, 213–226.

Bhattacharyya,A.A., Murchie,A.I.H., von Kitzing,E., Diekmann,S., Kemper,B. and Lilley,D.M.J. (1991) Model for the interaction of DNA junctions and resolving enzymes. *J. Mol. Biol.*, **221**, 1191–1207.

Birkenbihl,R.P. and Kemper,B. (1998a) Endonuclease VII has two DNA-binding sites each composed from one N- and one C-terminus provided from different subunits of the protein dimer. *EMBO J.*, **17**, 4527–4534.

Birkenbihl,R.P. and Kemper,B. (1998b) Localization and characterization of the dimerization domain of Holliday-structure resolving endonuclease VII. *J. Mol. Biol.*, **280**, 73–83.

Collaborative Computational Project No. 4 (1994) The CCP4 suite: programs for protein crystallography. *Acta Crystallogr.*, **D50**, 760–763.

Cowtan,K. (1994) 'dm': an automated procedure for phase improvement by density modification. *Joint CCP4 and ESF-EACBM Newsletter on Protein Crystallography*, **31**, 34–38.

de La Fortelle,E. and Bricogne,G. (1997) Maximum-likelihood heavy-atom parameter refinement for multiple isomorphous replacement and multiwavelength anomalous diffraction methods. *Methods Enzymol.*, **276**, 472–494.

Giraud-Panis,M.-J.E. and Lilley,D.M.J. (1996) T4 endonuclease VII: importance of a histidine–aspartate cluster within the zinc-binding domain. *J. Biol. Chem.*, **271**, 33148–33155.

Giraud-Panis,M.-J.E. and Lilley,D.M.J. (1997) Near-simultaneous DNA cleavage by the subunits of the junction-resolving enzyme T4 endonuclease VII. *EMBO J.*, **16**, 2528–2534.

Giraud-Panis,M.-J.E., Duckett,D.R. and Lilley,D.M.J. (1995) The modular character of a DNA junction resolving enzyme: a zinc binding motif in T4 endonuclease VII. *J. Mol. Biol.*, **252**, 596–610.

Golz,S., Birkenbihl,R.P. and Kemper,B. (1995) Improved large-scale preparation of phage T4 endonuclease VII overexpressed in *E.coli*. *DNA Res.*, **2**, 277–284.

Golz,S., Christoph,A., Birkenkamp-Demtröder,K. and Kemper,B. (1997) Identification of amino acids of endonuclease VII essential for binding and cleavage of cruciform DNA. *Eur. J. Biochem.*, **245**, 573–580.

Gopaul,D.N., Guo,F. and Van Duyne,G.D. (1998) Structure of the Holliday junction intermediate in Cre–*lox*P site-specific recombination. *EMBO J.*, **17**, 4175–4187.

Grebenshchikova,S.M.L., Plugina,L.A. and Shcherbakov,V.P. (1994) The role of T4-bacteriophage endonuclease VII in correction of mismatched regions. *Genetika*, **30**, 622–626.

Greger,B. and Kemper,B. (1998) An apyrimidinic site kinks DNA and triggers incision by endonuclease VII of phage T4. *Nucleic Acids Res.*, **26**, 4432–4438.

Guo,F., Gopaul,D.N. and Van Duyne,G.D. (1997) Structure of Cre recombinase complexed with DNA in a site-specific recombination synapse. *Nature*, **389**, 40–46.

Hickman,A.B., Waninger,S., Scocca,J.J. and Dyda,F. (1997) Molecular organization in site-specific recombination: the catalytic domain of bacteriophage HP1 integrase at 2.7 Å resolution. *Cell*, **89**, 227–237.

Iwasaki,H., Takahagi,M., Nakata,A. and Shinagawa,H. (1991) *Escherichia coli* RuvC protein is an endonuclease that resolves the Holliday structure. *EMBO J.*, **10**, 4381–4389.

Jones,T.A., Zou,J.-Y., Cowan,S.W. and Kjeldgaard,M. (1991) Improved methods for building protein models in electron density maps and the location of errors in these models. *Acta Crystallogr.*, **A47**, 110–119.

Kabsch,W. (1988) Evaluation of single-crystal X-ray diffraction data from a position-sensitive detector. *J. Appl. Crystallogr.*, **21**, 916–924.

Katayanagi,K., Miyagawa,M., Matsushima,M., Ishikawa,M., Kanaya,S., Ikehara,M., Matsuzaki,M. and Morikawa,K. (1990) Three-dimensional structure of ribonuclease H from *E.coli*. *Nature*, **347**, 306–309.

Kemper,B. (1997) Branched DNA resolving enzymes. In Nickoloff,J.A. and Hoekstra,M.F. (eds), *DNA Damage and Repair. Vol 1. DNA Repair in Prokaryotes and Lower Eukaryotes*. Humana Press Inc., Totowa, NJ, pp. 179–204.

Kemper,B. and Brown,D.T. (1976) Function of gene 49 of bacteriophage T4. II. Analysis of intracellular development and the structure of very fast-sedimenting DNA. *J. Virol.*, **18**, 1000–1015.

Kemper,B., Pottmeyer,S., Solaro,P. and Kosak,H. (1990) Resolution of DNA secondary structures by endonuclease VII (Endo VII) from phage T4. In Sarma,R.H. and Sarma,M.H. (eds), *Structure and Methods*. *Vol. 1. Human Genome Initiative and DNA Recombination.* Adenine Press, Schenectady, NY, pp. 215–229.

Kosak,H.G. and Kemper,B. (1990) Large scale preparation of T4 endonuclease VII from overexpressing bacteria. *Eur. J. Biochem.*, **194**, 779–784.

Kraulis,P.J. (1991) MOLSCRIPT: a program to produce both detailed and schematic plots of protein structures, *J. Appl. Crystallogr.*, **24**, 946–950.

Kupfer,C., Lee,S. and Kemper,B. (1998) Binding of endonuclease VII to cruciform DNA. *J. Biol. Chem.*, **273**, 31637–31639.

Kwon,H.J., Tirumalai,R., Landy,A. and Ellenberger,T. (1997) Flexibility in DNA recombination: structure of the lamda integrase catalytic core. *Science*, **276**, 126–131.

Lamzin,V.S. and Wilson,K.S. (1993) Automated refinement of protein models. *Acta Crystallogr.*, **D49**, 129–147.

Laskowski,R.A., MacArthur,M.W., Moss,D. and Thornton,J.M. (1993) PROCHECK—a program to check the stereochemical quality of protein structures. *J. Appl. Crystallogr.*, **26**, 283–293.

Mizuuchi,K., Kemper,B., Hays,J. and Weisberg,R.A. (1982) T4 endonuclease VII cleaves Holliday structures. *Cell*, **29**, 357–365.

Mueller,J.E., Newton,C.J., Jensch,F., Kemper,B., Cunningham,R.P., Kallenbach,N.R. and Seeman,N.C. (1990) Resolution of Holliday junction analogs by endonuclease VII can be directed by substrate structure. *J. Biol. Chem.*, **265**, 13918–13924.

Murchie,A.I.H. and Lilley,D.M.J. (1993) T4 endonuclease VII cleaves DNA containing a cisplatin adduct. *J. Mol. Biol.*, **233**, 77–85.

Murshudov,G.N., Vagin,A.A. and Dodson,E.J. (1997) Refinement of macromolecular structures by the maximum-likelihood method. *Acta Crystallogr.*, **D53**, 240–255.

Nicholls,A., Sharp,K.A. and Honig,B. (1991) Protein folding and association: insights from the interfacial and thermodynamic properties of hydrocarbons. *Proteins Struct. Funct. Genet.*, **11**, 281–296.

Otwinowski,Z. and Minor,W. (1997) Processing of X-ray diffraction data collected in oscillation mode. *Methods Enzymol.*, **276**, 307–326.

Parson,C.A., Kemper,B. and West,S.C. (1990) Interaction of a four-way junction in DNA with T4 endonuclease VII. *J. Biol. Chem.*, **265**, 9285–9289.

Pöhler,J.R.G., Giraud-Panis,M.-J. and Lilley,D.M.J. (1996) T4 endonuclease VII selects and alters the structure of the four-way DNA junction; binding of a resolution-defective mutant enzyme. *J. Mol. Biol.*, **260**, 678–696.

Pottmeyer,S. and Kemper,B. (1992) T4 endonuclease VII resolves cruciform DNA with nick and counter-nick and its activity is directed by local nucleotide sequence. *J. Mol. Biol.*, **223**, 607–615.

Roe,S.M., Barlow,T., Brown,T., Oram,M., Keeley,A., Tsaneva,I.R. and Pearl,L. (1998) Crystal structure of an octameric RuvA–Holliday junction complex. *Mol. Cell*, **2**, 361–372.

Schofield,M.J., Lilley,D.M.J. and White,M.F. (1998) Dissection of the sequence specificity of the Holliday junction endonuclease CCE1. *Biochemistry*, **37**, 7733–7740.

Solaro,P.C., Birkenkamp,K., Pfeiffer,P. and Kemper,B. (1993) Endonuclease VII of phage T4 triggers mismatch correction *in vitro*. *J. Mol. Biol.*, **230**, 868–877.

Subramanya,H.S., Arciszewska,L.K., Baker,R.A., Bird,L.E., Sherratt,D.J. and Wigley,D.B. (1997) Crystal structure of the site-specific recombinase, XerD. *EMBO J.*, **16**, 5151–5161.

Suck,D. (1994) DNA recognition by DNase I. *J. Mol. Recogn.*, **7**, 65–70.

Suck,D. (1998) DNA recognition by structure-selective nucleases. *Biopolymers*, **44**, 405–421.

Vassylyew,D.G., Kashiwagi,T., Mikami,Y., Ariyoshi,M., Iwai,S., Ohtsuka,E. and Morikawa,K. (1995) Atomic model of a pyrimidine dimer excision repair enzyme complexed with a DNA substrate: structural basis for damaged DNA recognition. *Cell*, **83**, 773–782.

Von Kitzing,E., Lilley,D.M.J. and Diekmann,S. (1990) The stereochemistry of a four-way DNA junction: a theoretical study. *Nucleic Acids Res.*, **18**, 2671–2683.

Vriend,G. (1990) What IF: a molecular modeling and drug design program. *J. Appl. Crystallogr.*, **28**, 347–351.

West,S.C. (1993) The nucleases of genetic recombination. In Linn,S.M., Lloyd,R.S. and Roberts,R.J. (eds), *Nucleases*. 2nd edn. Cold Spring Harbor Laboratory Press, Cold Spring Harbor, NY, pp. 145–170.

White,M.F. and Lilley,D.M.J. (1997) The resolving enzyme CCE1 of yeast opens the structure of the four-way DNA junction. *J. Mol. Biol.*, **266**, 122–134.

White,M.F., Giraud-Panis,M.-J., Pöhler,J.R.G. and Lilley,D.M.J. (1997) Recognition and manipulation of branched DNA structure by junction-resolving enzymes. *J. Mol. Biol.*, **269**, 647–664.

Youil,R., Kemper,B. and Cotton,R.G.H. (1995) Screening for mutations by enzyme mismatch cleavage with T4 endonuclease VII. *Proc. Natl Acad. Sci. USA*, **92**, 87–91.

Zhang,G. and Darst,S.A. (1998) Structure of the *E.coli* RNA polymerase α subunit amino-terminal domain. *Science*, **281**, 262–266.

Received December 7, 1998; revised and accepted January 19, 1999